

Supplementary Information

Thermochemical stability, electronic and dielectric properties of Janus bismuth oxyhalide materials BiOX (X = Cl, Br, I) monolayers

Tilak Das^{a,*} and Soumendu Datta^b

^a*Università degli Studi Milano-Bicocca, Dipartimento di Scienza dei Materiali, Via R. Cozzi, 55,
Milano - 20125, Italy*

^b*Department of Condensed Matter Physics and Material Sciences, Satyendra Nath Bose
National Centre for Basic Sciences, JD Block, Sector-III, Salt Lake City, Kolkata - 700
106, India*

**Email: tilak.das@unimib.it*

Content

Section S0: Phonon density of states calculations for pristine and Janus bismuth oxyhalide materials BiOX (X = Cl, Br, I) monolayers (ML)

Section S1: Electronic band structure of the BiOBr and BiOCl_{0.5}Br_{0.5} monolayers using PBE-D3 calculations

Section S2: Effective-mass calculation from second order derivative at extrema of valence and conduction bands

Section S3: Frequency dependent dielectric function, $\varepsilon(\omega)$ from PBE-D3+SO calculations

Section S4: Eliminating the contribution of the vacuum from dielectric constant, $\varepsilon_1(\omega = 0)$ from 3D periodic slab models

Section S0: Calculations of phonon density of states from pristine and Janus bismuth oxyhalide materials BiOX (X = Cl, Br, I) monolayers (ML)

The structural stability of these pristine BiOX (X= Cl, Br, I) and Janus BiO($X_{0.5}X'_{0.5}$ = Cl, Br, I) monolayers (ML) are rechecked from phonon calculations. Starting from the PBE-D3+SO optimized crystal structures we studied their phonon total density of states (DOS) based on the finite displacement technique in plane-wave based approach. Using the plane-wave DFT code VASP^{1,2,3}, the dynamical matrices for a given displacement 0.01Å on the lattices were calculated by the PBE-D3+SO formalism over the supercell of size 4×4×1 of the pristine or Janus monolayer with 6 atoms per unit cell. The force constants estimation and phonon DOS plots are done using the VASP and PHONOPY⁴ interface. More details of the VASP code based input for force and energy convergence during the single self consistent runs are given in the methodology section of the manuscript (see **Section 2**). During the phonon DOS calculations, we have estimated that 32×32×64 irreducible q -points sampling mesh and Gauss broadening 0.1 THz was sufficient to reach the required convergence. In **Figure S1**, the calculated phonon total DOS of one pristine model i.e. ML-BiOCl (top left) and in other panels DOS of Janus ML-BiO($X_{0.5}X'_{0.5}$ = Cl, Br, I) are shown.

It is very much obvious that the pristine ML-BiOCl shows clear dynamical stability as similar to the earlier reported theoretical investigation (see more detail in the main manuscript, **Section 3.2**), thus validate our current computational approach. Continuing with the same level of the theoretical formulation PBE-D3+SO, very interestingly we have found that the structural stability for the two Janus models i.e. ML-BiO($Cl_{0.5}Br_{0.5}$) and ML-BiO($Br_{0.5}I_{0.5}$). However, the minor negative frequency is observed for the Janus ML-BiO($Cl_{0.5}I_{0.5}$), which is possibly due to the larger mismatch of the Cl and I atom sizes within the ultrathin layers of bismuth oxyhalides. Thus, we emphasize here that the present monolayers are expected to be technologically robust and would be feasible for future clean synthesis from experimental.

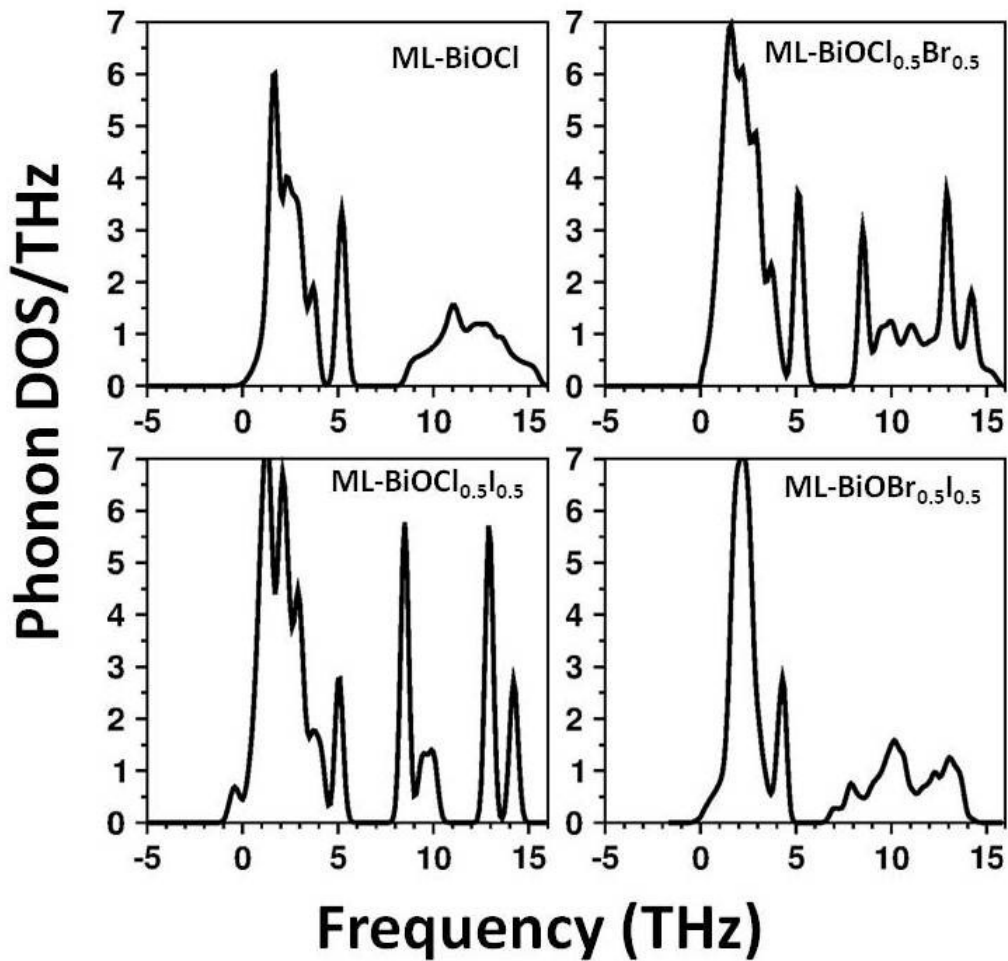


Figure S1: Calculated phonon density of states (DOS), for pristine BiOCl and Janus BiO($X_{0.5}X'_{0.5}$ = Cl, Br, I) monolayers at PBE-D3+SO calculations on their full optimized crystal structures.

Section S1: Electronic band structure of the BiOBr and BiOCl_{0.5}Br_{0.5} monolayers using PBE-D3 functional calculations

The robustness of our calculated indirect electronic transitions which is observed for the monolayers ML-BiOBr and ML-BiO($Cl_{0.5}Br_{0.5}$), are also validated from the present PBE-D3 computations. In the **Figure S2**, we have given their electronic total band structure plots from the PBE-D3 calculations in panel a) and b), respectively. The calculated indirect bands gap for the pristine ML-BiOBr is 2.41 eV and for Janus ML-BiO($Cl_{0.5}Br_{0.5}$) is 2.48 eV. Indeed, at these first-principles PBE-D3 or PBE-D3+SO levels of computation the nature

of this particular type of indirect bands transitions are always present for these two materials, independent of the choice of spin-orbit (SO) effect. Specifically, a moderate amount of the SO effect is thus observed, because the indirect band gap reduced by 0.10-0.15 eV at PBE-D3+SO level calculations which were 2.30 and 2.34 eV respectively for ML-BiOBr and ML-BiO($Cl_{0.5}Br_{0.5}$).

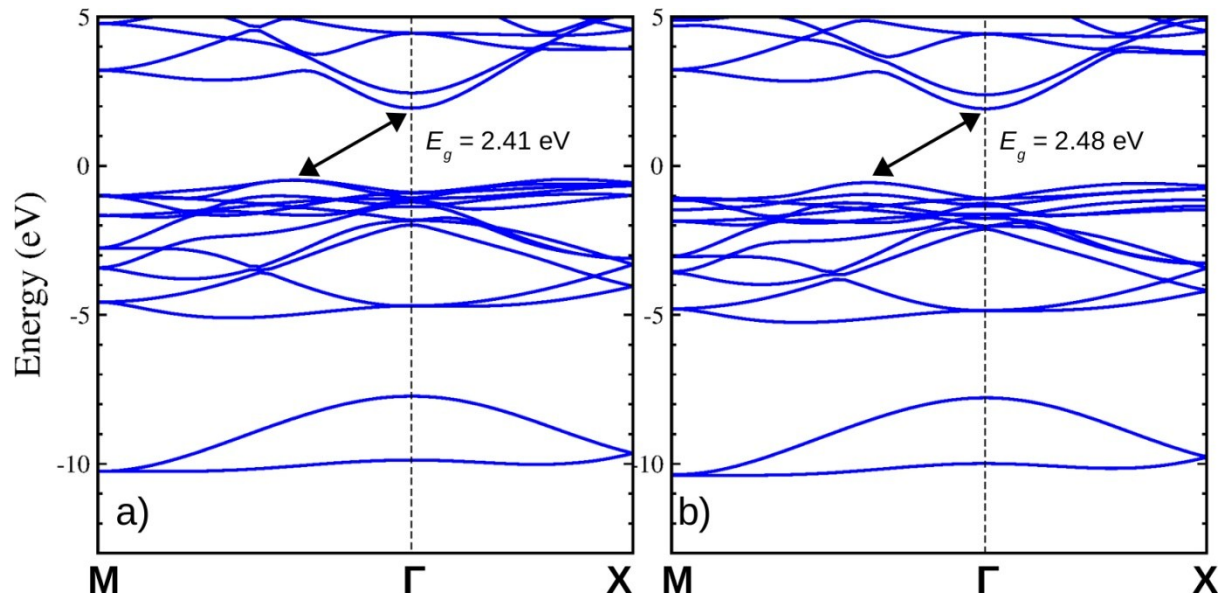


Figure S2: At PBE-D3 level computed electronic band structure of the ML-BiOBr and ML-BiO($Cl_{0.5}Br_{0.5}$), respectively in panel a) and b). The indirect transitions are marked with double headed black line arrow in each plot. The indirect band gap, E_g is also marked in each plots. The Fermi level is set to zero of the Energy axis ($E_F = 0$).

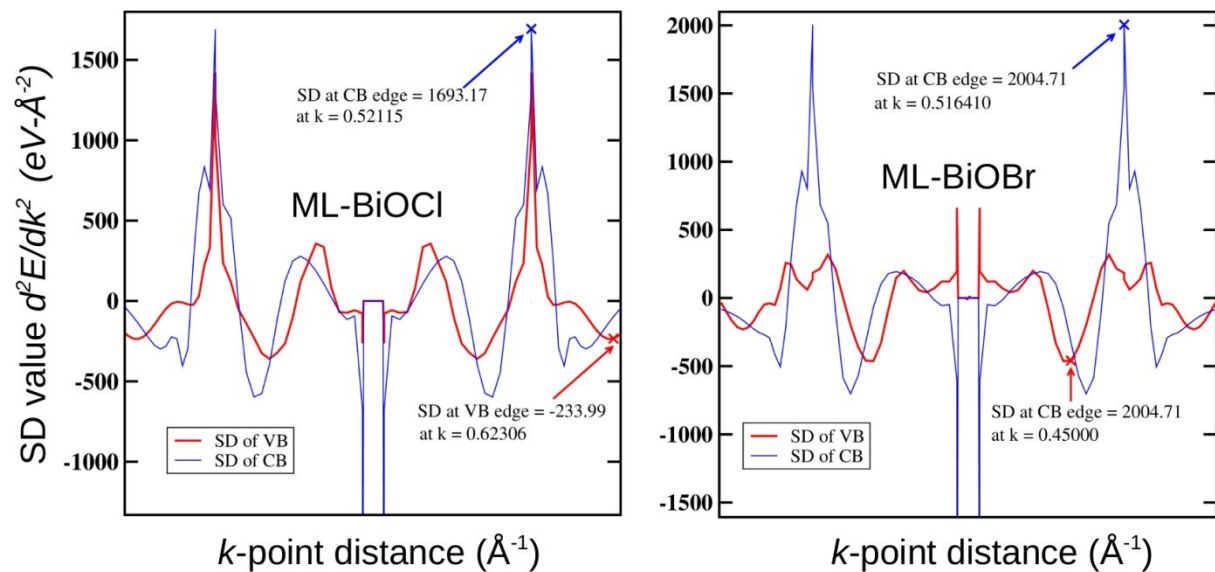
Section S2: Effective-mass calculation from second order derivative at extrema of valence and conduction bands

Newton's Second Law of motion has been widely used for the classical particles, which is equivalent to the independent electron and hole motion within the electronic band-structure of solids, as derived from the semilocal Kohn-Sham theory. Thus, from the mobility the mass of the charge carriers can be derived. The mobility of the charge carriers are inversely proportional to the effective-mass (m^*) of these charge carriers in semiconductors and insulators in common practice. Thus, the measure of the second order derivative (SD) at the conduction band (CB) and valence band (VB) band-edges are essential to get an

estimation of the electron and hole effective masses, respectively at the given k -point of the Brillouin zone of the at conduction and valence band, respectively. The central difference method was used for the numerical differentiation to obtain the SD values. In the various cases of pristine BiOX and Janus BiO $X_{0.5}X'_{0.5}$ monolayer materials, we have estimated this second order derivative of energy eigenvalue (E) at the given k -point k in the k -space of the given lattice, as obtained from electronic band-structure within PBE-D3+SO functional calculations and effective-mass are estimated using the following, equation (1):

$$m^* = \hbar^2 \left[\frac{d^2E}{dk^2} \right]^{-1} \dots \dots \dots (1)$$

Here \hbar is the reduced Planck constant, and in common use this effective masses are expressed in terms of the rest mass of the electron m_0 . In our all studies monolayers models we have given the marked second order derivative values in each plots of within **Figure S3**.



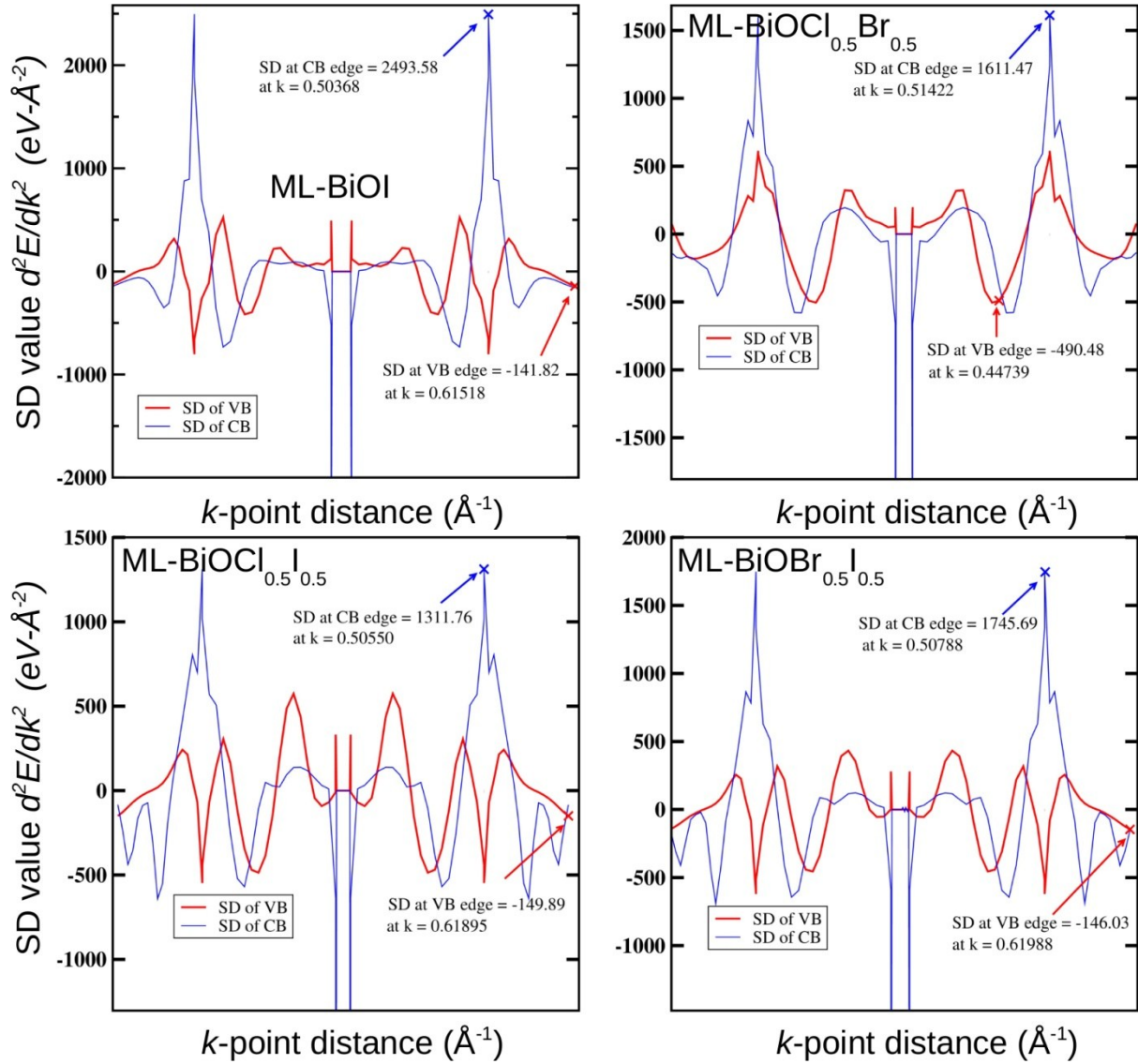


Figure S3: At PBE-D3+SO level in all three rows, are given for the pristine BiOX and Janus $\text{BiO}X_{0.5}X'_{0.5}$ ($X, X' = \text{Cl}, \text{Br}, \text{I}$) monolayers. The second derivative (SD) of the last occupied valence band (VB) and first empty conduction band (CB) are marked in each plot with red and blue solid lines, respectively for all cases. A cross mark is used at the VB and CB band-edges, respectively with red and blue color where SD was taken and their values are printed at the given k -point.

Section S3: Frequency dependent dielectric function, $\epsilon(\omega)$ from PBE-D3+SO calculations

The Real, $\epsilon_1(\omega)$ and Imaginary, $\epsilon_2(\omega)$ component of the frequency dependent dielectric function from the density functional perturbation theory are computed. We have used the PBE-D3 functional including the spin-orbit effect (SO). The computed spectrums are shown in the **Figure S4** and **S5**.

For both the pristine BiOX (cf. **Figure S4**) and Janus $\text{BiO}^{X_{0.5}X'_{0.5}}$ (cf. **Figure S5**) monolayers the in-plane, ϵ^{\parallel} and out-of-plane, ϵ^{\perp} component are marked with Red dashed (or black solid) lines and green solid lines, respectively. Due to tetragonal symmetry, we have clearly seen the presence of degenerate component in-plane and moderate optical anisotropy present for the out-of-plane component.

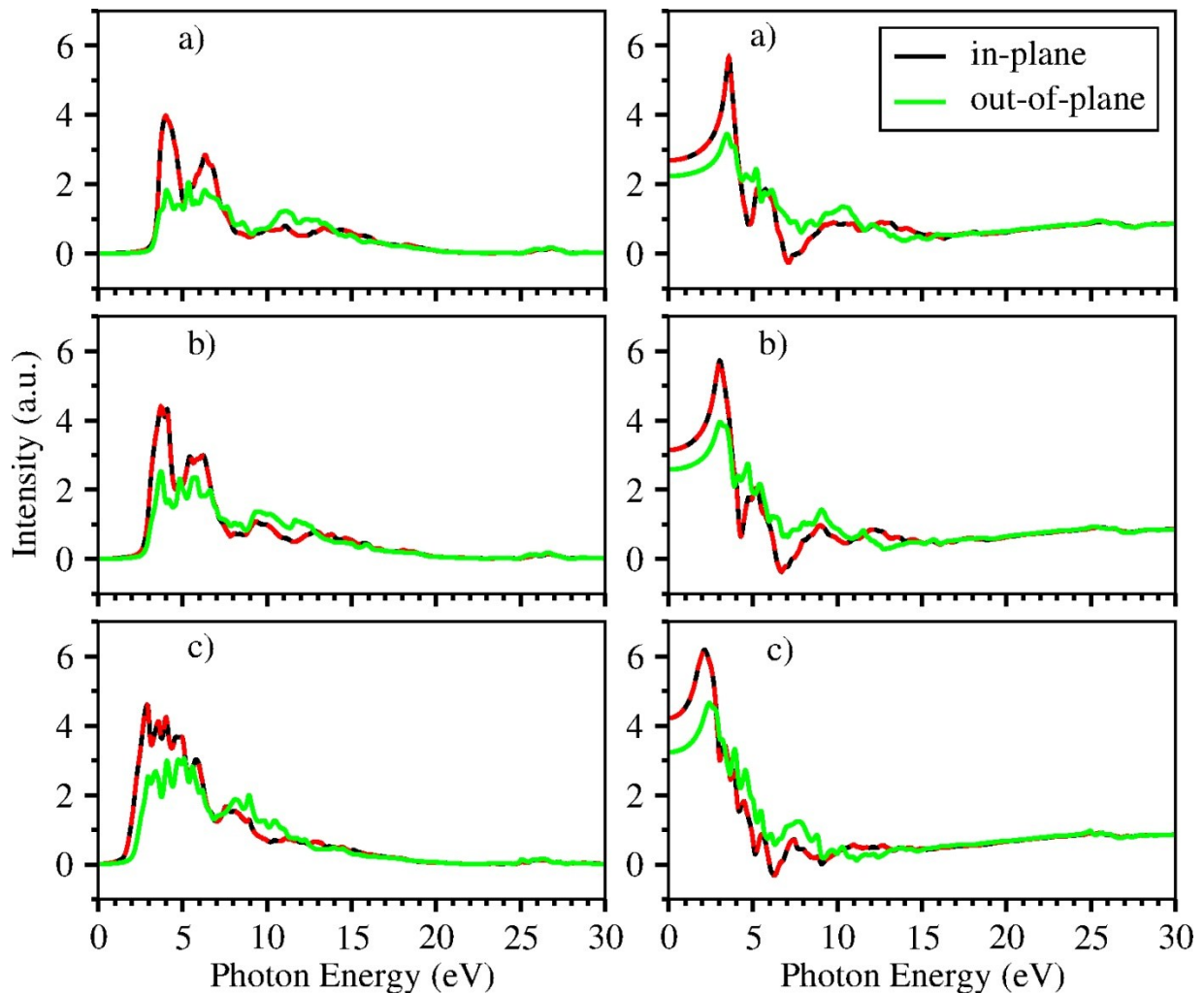


Figure S4: Computed using PBE-D3+SO theoretical level of Imaginary (left panels a, b, and

c) and Real (right side panels a, b, and c) part of dielectric function of pristine BiOX monolayers (ML) with X = Cl, Br, I.

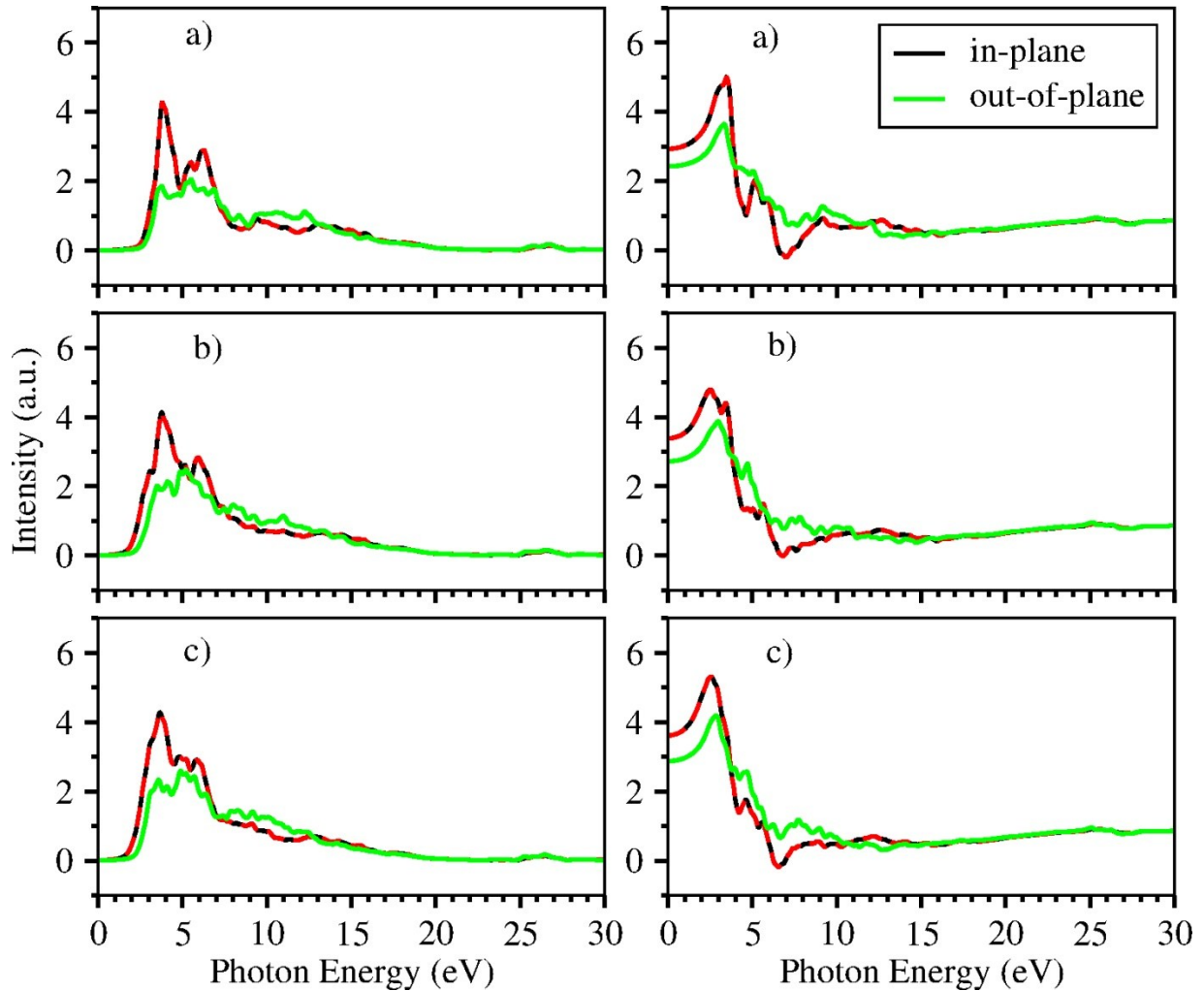


Figure S5: Computed using PBE-D3+SO theoretical level of Imaginary (left panels a, b, and c) and Real (right side panels a, b, and c) part of dielectric function of Janus $\text{BiO}^{X_{0.5}X'_{0.5}}$ monolayers (ML) with $X, X' = \text{Cl, Br, I}$.

Section S4: Eliminating the contribution of the vacuum from dielectric constant, $\epsilon_1(\omega = 0)$ from 3D periodic slab models

The limitation of the computed dielectric constants values using density functional perturbation theory (DFPT) from a pseudo three dimensional (3D) model *i.e.* model using certain amount of vacuum for the slab calculations using plane-wave periodic code VASP⁵, has been recently discussed in the recent work by A. Laturia *et al.* 2018.⁶ According to this study, the contribution of the vacuum should be eliminated from principle of capacitance of 3D supercell, in order to get values for real 2D slab material. The in-plane, ϵ_1^{\parallel} and out-of-plane, ϵ_1^{\perp} values are written as the parallel and series combination of the 2D-slab material and vacuum regions as two capacitors to get the capacitance of the pseudo 3D periodic supercell. For the given supercell out-of-plane lattice parameter c , and 2D-slab materials width $d_{x-x(x')}$ the in-plane and out-of-plane dielectric constant values for the 2D-slab model is written in terms of the 3D periodic supercell model calculated values, of $\epsilon_1^{\parallel s}$ and $\epsilon_1^{\perp s}$, respectively with following equations (2) and (3):

$$\epsilon_1^{\parallel} = \frac{c}{d_{x-x(x')}} (\epsilon_1^{\parallel s} - 1) + 1 \quad \dots\dots\dots (2)$$

$$\frac{1}{\epsilon_1^{\perp}} = \frac{c}{d_{x-x(x')}} \left(\frac{1}{\epsilon_1^{\perp s}} - 1 \right) + 1 \quad \dots\dots\dots (3)$$

We have calculated the values of $\epsilon_1^{\parallel s}$ and $\epsilon_1^{\perp s}$ from our theoretical formulation using PBE-D3 and PBE-D3+SO (SO: Spin orbit effect) calculations from the pseudo 3D supercell model were used to calculate the values in the 2D-slab model for all pristine and Janus monolayer of the bismuth oxyhalides. The effect of the local field effect is also included via Random Phase Approximation.^{7,8} Details of all parameters are given in the **Table S1**.

Table S1: PBE-D3 and PBE-D3+SO functional computed average static dielectric constant,

with and without LFE correction, $\epsilon_{1avg}(\omega = 0) = \frac{1}{3}(\epsilon_1^{\perp} + 2\epsilon_1^{\parallel})$ of ultrathin films of pristine BiOX and Janus BiO^X0.5X'^{0.5} monolayers material, where ϵ_1^{\perp} and ϵ_1^{\parallel} are out-of-plane and in-plane dielectric constants, respectively and ω is photon frequency.

	ϵ_1^{\parallel}	ϵ_1^{\perp}	$\epsilon_{1avg}(\omega =$	ϵ_1^{\parallel}	ϵ_1^{\perp}	3D cell $c-$	Width	$\epsilon_{1avg}(\omega =$
--	--------------------------	----------------------	----------------------------	--------------------------	----------------------	--------------	-------	----------------------------

Materials (Methods)	(3D)	(3D)	in 3D	(2D)	(2D)	parameter (Å)	$d_{x-x'}$ (Å)	in 2D
BiOCl	PBE-D3							
(No-LFE)	2.61	2.22	2.48	9.12	-0.56	27.23	5.40	5.89
(LFE-RPA)	2.41	1.28	2.03	8.11	-9.70	27.23	5.40	2.17
	PBE-D3+SO							
(No-LFE)	2.71	2.24	2.55	9.61	-0.56	27.19	5.40	6.22
(LFE-RPA)	2.50	1.28	2.09	8.55	-9.86	27.19	5.40	2.42
BiOBr	PBE-D3							
(No-LFE)	3.15	2.50	2.93	11.02	-0.56	26.88	5.77	7.16
(LFE-RPA)	2.89	1.33	2.37	9.80	-6.41	26.88	5.77	4.40
	PBE-D3+SO							
(No-LFE)	3.25	2.58	3.03	11.34	-0.55	26.55	5.78	7.37
(LFE-RPA)	2.98	1.34	2.43	10.09	-6.04	26.55	5.78	4.42
BiOI	PBE-D3							
(No-LFE)	3.81	3.02	3.55	12.89	-0.55	26.28	6.21	8.41
(LFE-RPA)	3.46	1.41	2.78	11.41	-4.34	26.28	6.21	6.16
	PBE-D3+SO							
(No-LFE)	4.28	3.21	3.92	14.52	-0.54	25.68	6.23	9.50
(LFE-RPA)	3.87	1.42	3.06	12.83	-4.56	25.68	6.23	7.03
BiOCl_{0.5}Br_{0.5}	PBE-D3							
(No-LFE)	2.79	2.36	2.65	9.69	-0.56	27.09	5.58	6.27
(LFE-RPA)	2.56	1.30	2.14	8.57	-8.31	27.09	5.58	2.95
	PBE-D3+SO							
(No-LFE)	2.94	2.43	2.77	10.26	-0.55	26.88	5.63	6.66
(LFE-RPA)	2.70	1.31	2.24	9.12	-7.70	26.88	5.63	3.51
BiOCl_{0.5}I_{0.5}	PBE-D3							
(No-LFE)	3.21	2.63	3.02	11.14	-0.54	26.67	5.81	7.25
(LFE-RPA)	2.93	1.34	2.40	9.86	-6.07	26.67	5.81	4.55
	PBE-D3+SO							
(No-LFE)	3.41	2.71	3.18	11.98	-0.53	26.56	5.83	7.81
(LFE-RPA)	3.12	1.35	2.53	11.66	-5.52	26.56	5.83	5.27
BiOBr_{0.5}I_{0.5}	PBE-D3							
(No-LFE)	3.40	2.77	3.19	11.63	-0.55	26.52	5.99	7.57
(LFE-RPA)	3.09	1.37	2.52	10.25	-5.11	26.52	5.99	5.13
	PBE-D3+SO							
(No-LFE)	3.64	2.86	3.38	12.66	-0.53	26.49	6.00	8.26
(LFE-RPA)	3.32	1.37	2.67	11.24	-5.20	26.49	6.00	5.76

References

- ¹ G. Kresse, and J. Hafner, *Phys. Rev. B*, 1993, **47**, 558-561.
- ² G. Kresse, and J. Furthmüller, *Comput. Mater. Sci.*, 1996, **6**, 15.
- ³ G. Kresse, and D. Joubert, *Phys. Rev. B*, 1999, **59**, 1758-1775.
- ⁴ A. Togo and I. Tanaka, *Scr. Mater.*, 2015, **108**, 1-5.
- ⁵ M. Gajdos, K. Hummer, G. Kresse, J. Furthmüller and F. Bechstedt, *Phys. Rev. B*, 2006, **73**, 045112.
- ⁶ A. Laturia, M. L. Van de Put, and W. G. Vandenberghe, *npj 2D Materials and Applications*, 2018, **2(6)**, 1-6.
- ⁷ S. Baroni, and R. Resta, *Phys. Rev. B*, 1986, **33**, 7017.
- ⁸ G. Kresse, and J. Furthmüller, *Phys. Rev. B*, 1996, **54**, 11169-11186.